Published in final edited form as:
Epilepsia. 2010 August ; 51(8): 1587–1597. doi:10.1111/j.1528-1167.2009.02420.x.

Spatiotemporal patterns of electrocorticographic very fast oscillations (>80 Hz) consistent with a network model based on electrical coupling between principal neurons

Roger D. Traub[*], **Roderick Duncan**[†], **Aline J.C. Russell**[†], **Torsten Baldeweg**[‡], **Yuhai Tu**[*], **Mark O. Cunningham**[§], and **Miles A. Whittington**[§]

[*]Department of Physical Sciences, IBM T.J. Watson Research Center, Yorktown Heights, New York, U.S.A.

[†]Department of Clinical Neurophysiology, Institute of Neurological Sciences, Southern General Hospital, Glasgow, United Kingdom

[‡]Institute of Child Health, University College London, London, United Kingdom

[§]Institute of Neuroscience, The Medical School, Framlington Place, Newcastle University, Newcastle, United Kingdom

SUMMARY

Purpose—We sought to characterize spatial and temporal patterns of electrocorticography (ECoG) very fast oscillations (> ~80 Hz, VFOs) prior to seizures in human frontotemporal neocortex, and to develop a testable network model of these patterns.

Methods—ECoG data were recorded with subdural grids from two preoperative patients with seizures of frontal lobe onset in an epilepsy monitoring unit. VFOs were recorded from rat neocortical slices. A "cellular automaton" model of network oscillations was developed, extending ideas of Traub et al. (*Neuroscience*, 92, 1999, 407) and Lewis & Rinzel (*Network: Comput Neural Syst*, 11, 12000, 299); this model is based on postulated electrical coupling between pyramidal cell axons.

Results—Layer 5 of rat neocortex, in vitro, can generate VFOs when chemical synapses are blocked. Human epileptic neocortex, in situ, produces preseizure VFOs characterized by the sudden appearance of "blobs" of activity that evolve into spreading wavefronts. When wavefronts meet, they coalesce and propagate perpendicularly but never pass through each other. This type of pattern has been described by Lewis & Rinzel in cellular automaton models with spatially localized connectivity,

Address correspondence to Roger D. Traub, M.D., Department of Physical Sciences, IBM T.J. Watson Research Center, 1101 Kitchawan Road, Yorktown Heights, NY 10598, U.S.A. rtraub@us.ibm.com.

Disclosures

The authors have no conflicts of interest to report.

Additional Supporting Information may be found in the online version of this article:

There are two videos, expanding on the ECoG and simulation data in Fig. 2. Each video lasts 50 s and represents 250 ms of data (i.e., the videos are slowed 200-fold relative to real time). In addition, there is an Appendix with four figures, providing details concerning the cellular automaton model.

Appendix S1. Properties of the cellular automaton model

Video S1

Video S2

Please note: Wiley-Blackwell is not responsible for the content or functionality of any supporting materials supplied by the authors. Any queries (other than missing material) should be directed to the corresponding author for the article.

and is demonstrated here with 120,000- to 5,760,000-cell models. We provide a formula for estimating VFO period from structural parameters and estimate the spatial scale of the connectivity.

Discussion—These data provide further evidence, albeit indirect, that preseizure VFOs are generated by networks of pyramidal neurons coupled by gap junctions, each predominantly confined to pairs of neurons having somata separated by < ~1–2 mm. Plausible antiepileptic targets are tissue mechanisms, such as pH regulation, that influence gap-junction conductance.

Keywords

Ripple; Gap junction; Cellular automaton

Numerous authors have reported the occurrence of very fast field potential/electroencephalography (EEG)/electrocorticography (ECoG) oscillations, at frequencies ≥80 Hz, prior to, during, and after paroxysmal epileptic events (either interictal or ictal), and both in patients and in experimental preparations, in vivo and in vitro (references include, but are not limited to: Fisher et al., 1992; Bragin et al., 1999a,b, 2002; Grenier et al., 2001, [2003]; Jacobs et al., 2008; Khosravani et al., 2009; Worrell et al., 2004; Traub 2et al., 2001, 2005; Roopun et al., in prep.) In some cases, VFOs appear to arise in exquisitely localized regions of cortical tissue (Bragin et al., 1999b, 2002; Roopun et al., in 3prep.); sometimes other epileptiform events can also arise in highly localized regions (Schevon et al., 2008). On different occasions, however, VFOs occur simultaneously in a number of subdural grid ECoG electrodes (e.g., Fig. 1 of Traub et al., 2001), and such activity presumably encompasses several squared centimeters of cortical surface. Although VFOs may be useful in identifying seizure-onset zones (Roopun et al., 2009), it is interesting to note that VFO occurrence is not specific to particular pathologies, and it is not directly related to local pathologic changes (Jacobs et al., 2008). These latter observations suggest that the ability to generate VFOs might be a normal facet of cortical function, which is pathologically enhanced in epilepsy.

To our knowledge, the detailed spatiotemporal patterns of VFOs have not yet been investigated. There also continues to be uncertainty concerning the cellular mechanisms of different sorts of VFOs and their significance for epileptogenesis (Engel et al., 2009). Clearer understanding of the two related issues—VFO spatiotemporal pattern and cellular mechanism—may have clinical importance: Factors in the brain that predispose to VFO may also predispose to seizures, or VFO itself may promote seizure onset.

In our view, the evidence that in vitro VFO is generated by gap junctional coupling between principal neurons is compelling. The evidence is both positive and negative. On the positive side: Such VFO occurs when chemical synaptic transmission is globally suppressed with low-Ca^{2+} media, or selectively suppressed with blockers of particular synaptic receptors, including γ-aminobutyric acid $(GABA)_A$ receptors; in vitro VFO is associated with action potentials and spikelets in pyramidal cells that are phase-locked to field VFO and it is suppressed by carbenoxolone, halothane, and octanol, all blockers of gap junction conductance, and is augmented by alkalinization of the medium, which would open most types of gap junctions (Draguhn et al., 1998; Nimmrich et al., 2005; Roopun et al., in prep.—but see Gonzáles-Nieto et al., 2008). Furthermore, a detailed network model, based on postulated gap junctional coupling between pyramidal cell axons, produces field and intracellular potentials closely resembling experiment (Traub et al., 1999; see also Fig. 1). (The evidence that such gap junctions actually exist is reviewed in the Discussion.) On the *negative* side, we are not aware of any cortical experimental preparation, dependent on chemical synapses, that has been shown to generate network oscillations at the requisite frequencies.

With respect to in vivo epilepsy-related VFOs, Grenier et al. (2003) reported that the gap junction blocker halothane suppressed both the VFOs and seizures that spontaneously occurred

in ketamine–xylazine anesthetized cats. However, the cellular mechanisms of in vivo VFO are difficult to study experimentally, at least in a direct fashion. For example, although intracellular and juxtacellular recordings are possible in vivo (in experimental animals), blockade of synaptic transmission is hard to achieve. There is a useful role for network models in a situation such as this, as such models can suggest novel experiments that may be practical to perform.

Detailed neuronal network models, of the sort mentioned in the preceding and used to simulate VFOs, are computationally intensive. The original one (Traub et al., 1999) involved <4,000 hippocampal pyramidal neurons simulated on a parallel computer. Although we are now able to simulate up to 15,000 detailed cortical pyramidal cells (see subsequent text), that number is still not sufficient to study complex spatiotemporal VFO patterns. We proposed a drastic reduction of the computational complexity (Traub et al., 1999), by using a cellular automaton model, in which each neuron, and the rules for neuron–neuron interaction, are greatly simplified. Cellular automaton models lend themselves to large simulations, adequate to illustrate spatiotemporal patterns. Our original conceptual framework was in the context of random graphs (i.e., randomly connected networks) (Erdös & Rényi, 1960). However, Lewis and Rinzel (2000) examined cellular automaton models in which the "gap junctional" connectivity between model neurons was spatially localized (that is, not globally random, rather only locally random), whereas the network size was large relative to the localization scale. Lewis and Rinzel showed that in such a situation, traveling waves were produced, as in an excitable medium, even when gap junctional connectivity was sparse (as it is expected to be from dye-coupling data (Gutnick et al., 1985); and furthermore, different waves have a characteristic type of interaction (coalescence) when they meet.

In the present study, we demonstrate that this wave-like behavior—generated by a large cellular automaton model based on the postulate of axonal electrical coupling—characterizes the spatiotemporal patterns of VFO activity recorded prior to seizures in select epileptic patients. The data additionally support the notion that each wave of VFO is initiated in a localized cortical region. Having a model that accounts for both temporal and spatial aspects of VFO lends support to the model's postulate of gap junctions between principal neurons. Such a postulate, in turn, has concrete implications for novel approaches to the care of patients with epilepsy.

Methods

Patient recordings

We analyzed ECoG data from two preoperative patients with epilepsy who had subdural grids placed as part of their presurgical evaluation. All recordings were carried out with proper informed consent and the approval of the local ethics committees.

The ECoG data illustrated in this report derived from "Patient B" of Roopun et al. (2009) (see subsequent text). Recordings were made with 6 × 8-contact subdural grid (Ad-Tech Medical Instrument Corp., Racine, WI, U.S.A., http://www.adtechmedical.com), containing platinum. Contacts were 1 cm apart, 4 mm in diameter, 0.7 mm deep, and had a 2.3 mm diameter exposed surface. For the other patient ["Patient 1" of Traub et al. (2001)], a 4 × 8-contact subdural grid (Ad-Tech) was used, with 1 cm interelectrode spacing, and 2.3 mm diameter exposed surface on the platinum contact. Recordings were made using either NeuroScan 6or Xltek equipment with output bandwidth up to 500– 1,000 Hz. Reference was to a distant contact on the subdural strip, and was then re-referenced to a common average signal.

Data analysis

All clinical datasets were resampled at 2 kHz, and band-pass filtered at 70–500 Hz, using a finite impulse response filter with zero-phase distortion. Epochs of VFO thus treated were then normalized across all channels for peak amplitude. The resulting spatiotemporal pattern of activity was plotted using a color map with sharp min/max transition at zero volts, to illustrate the progress of the wavefronts. All analysis was performed in the Mat lab environment (The Mathworks Inc., Natick, MA, U.S.A.)

In vitro neocortical slice experiments

Horizontal slices of temporal neocortex (450 μm thick) were prepared from adult male Wistar rats (150–250 g), according to Roopun et al. (2006). All procedures were performed in accordance with the UK Home Office Animals (Scientific Procedures) Act, 1986. Slices were maintained at 34°C, at the interface between warm wetted 95% O_2/5% CO_2 and aCSF (artificial cerebrospinal fluid) containing (in mM): 3 KCl, 1.25 NaH_2PO_4, 1 $MgSO_4$, 1.2 $CaCl_2$, 24 $NaHCO_3$, 10 glucose, and 126 NaCl. Extracellular recordings from layer 5 were obtained using glass micropipettes containing the above aCSF (resistance <0.5 MΩ). Intracellular recordings from intrinsically bursting somata in layer 5 were taken with sharp microelectrodes filled with potassium acetate (resistance 30–90 MΩ). Signals were analog filtered at 2 kHz and digitized at 10 kHz. Fast synaptic events were blocked with a cocktail of drugs containing SYM2206 7 (20 mM, to block AMPA receptors), d-APV [50 mM, to block *N*-methyl-D-aspartate (NMDA) receptors], and gab-azine (0.5 mM, to block most $GABA_A$ receptors). Kainate (400 nM) was used to activate oscillations. All drugs were obtained from Tocris, United Kingdom. Transient runs of VFOs were induced by pressure ejection of aCSF (composition as noted previously) containing the drug cocktail, and pH adjusted to 8.5 with NaOH. The volume of solution ejected on layer 5 was 70–200 nl.

Detailed network simulations

We developed a simulation program based on the thalamocortical column model described in Traub et al. (2005), with this major difference: The only cell type now simulated was the layer 5 tufted intrinsically bursting (IB) pyramidal cell, of which there were now 15,000. Each model neuron had, as before, 61 compartments: a soma; a 6-compartment axon; and 54 compartments for the basal, oblique, and apical dendrites. There were multiple voltage-dependent and Ca^{2+}-dependent membrane conductances, although for the sake of simplicity, high-threshold g_{Ca} and $g_{K(AHP)}$ were blocked.

The model neurons were interconnected by axonal gap junctions, in a globally random topology, with an average of 3.33 gap junctions on each neuron (written as <i> = 3.33, the symbol standing for “mean index”). Gap junction conductance was 7 nS in the example illustrated below, which would usually permit an action potential to cross from one firing axon to a coupled other axon. Random (i.e., following independent Poisson statistics) current pulses were delivered to each axon at an average frequency of 4 Hz; such pulses would cause “ectopic spikes” when the cell was not refractory from a recent spike. There were no chemical synapses.

The program stored membrane potentials at various locations (axon, soma, apical dendrite) of selected neurons, as well the estimated field potential, the units of which are arbitrary. The method for estimating field potentials is described in Traub et al. (2005).

Each run of the program simulated 1 s of neural activity. The program ran on 40 processors of an IBM Linux cluster, and required approximately 36 h to complete. Code was written in Fortran and run in the mpi parallel environment. Cellular automaton code (see below) was also written in Fortran. Smaller models ran on a single processor of an IBM 7040-681 AIX parallel machine, whereas the largest model (5.76 million cells) ran on 20 processors of the same

computer, again in the mpi parallel environment. All source code is available upon writing to rtraub@us.ibm.com.

Cellular automaton model

Cellular automata ("CA") (Sarkar, 2000; Wolfram, 2002) have been used to model a number of phenomena and processes in mathematics and physics, including the behavior of gases, galactic structure (Seiden et al., 1979), and neuronal networks (Pytte et al., 1991). First, we describe the simplest form of CA—finite deterministic—and then describe the stochastic modification actually used in the report.

A finite, deterministic (synchronous) CA consists of a finite number of elements, here called "cells" to suggest the biologic connection, where

1. each cell has inputs from a specific set of other cells:
2. each cell can exist in a finite number of states, the list of states being the same for all cells;
3. time is discrete, and cells change states synchronously every time step;
4. there is a rule—the same for all the cells—that determines how cells change states: the rule has the property that state changes, for each cell, depend only on the present state of the respective cell, and the present states of cells supplying input to the respective cell.

With the stochastic modification that we use, the state-change rule also allows cells that are in a particular state, to switch states randomly, according to a defined statistical rule. This stochastic property corresponds biologically to the possibility of a spontaneous action potential occurring in an axon, perhaps as a result of fluctuations in Na^+ channel openings.

The "inputs" in the CA model correspond to connections mediated by nonrectifying gap junctions, and are, therefore, assumed symmetrical: If cell A receives input from cell B, then B receives input from A. The states will correspond to "firing," various stages of "refractoriness," and "excitable"—that is, available to be excited if a connected cell is firing, or if a spontaneous event occurs. The discrete time step in the CA model corresponds physically to the shortest relevant time interval for VFOs: the time it takes for a spike in one axon to evoke a spike in a coupled axon (this time, in the actual brain, will depend on gap junction conductance, intrinsic membrane properties, and other quantities). We shall assume that the discrete time step in the CA model corresponds, physically, to 0.25 ms, which is biologically reasonable (Mercer et al., 2006). The CA rule for changing the states of cells will incorporate the idea, from membrane biophysics, that after a cell fires, it is refractory for a short time, and then available to fire again. (The CA model used here is too simple to incorporate those details of membrane kinetics that actually govern refractoriness.)

More formally, the CA model is built, and behaves, as follows:

1. Cells are usually organized into a two-dimensional ("2D") array, either 400 × 300 (120,00 cells), or 800 × 600 (480,000 cells). The unit spacing in the array will be called the "lattice spacing"; what physical dimensions to which the lattice spacing corresponds will be considered in the Discussion. The shape of the array, with one side = 3/4 × the other side, was chosen to correspond to the 6 × 8 subdural grid of electrodes used in patients. In some simulations, we used a larger 3D array, with dimensions 1,600 × 1,200 × 3, containing a total of 5,760,000 cells. Note that the clinical ECoG data available to us are effectively 2D, motivating our preferred use of 2D model arrays; 3D arrays were tested for the sake of completeness.

2. The statistical properties of the connectivity are defined by two parameters: (a) the total number of connections (i.e., "gap junctions"), or alternatively <i>, the mean index; for the simulations illustrated in this article, <i> = 1.33, a sparse degree of connectivity; and (b) a parameter c_r, called by Lewis and Rinzel (2000) the "footprint." Two cells are allowed to be connected to each other if, and only if, they are at most c_r lattice spacings apart. (Of course, two nearby cells will, in general, not be connected: Only some allowable pairs actually have connections.) When $c_r = \infty$, the graph is "globally random." In this case, the only parameter determining connectivity is the mean index, <i> (c.f. Erdö s & Rényi, 1960, who use a different notation, namely what they call "c," equal to 0.5 × <i>). c_r is a critical parameter for our model, determining whether waves of activity exist, and how fast they will propagate. For the 3D model, c_r depends only on separation in the x–y plane (1,600 × 1,200), and not along the z axis.

3. Each cell can exist in any of 17 possible states, which we may call "*firing*" (or "*on*"); "*excitable*"; and 15 refractory states, called $refr_1$, $refr_2$,…, $refr_{15}$. (Thus, the total refractoriness will be 15× the time step = 15 × 0.25 ms = 3.75 ms.) The refractoriness was made this long to prevent epochs of reentrant rhythms caused by activity propagating around short cycles in the network, leading to extremely high-frequency stereotypical activity (Lewis & Rinzel, 2000).

4. The dynamics, that is, the rules for changing states, can be divided into two parts. The *first* part is, in a sense, trivial: It consists of state changes that are "forced," that is, that do not depend on inputs to the respective cell. These state changes are: *firing* → $refr_1$; $refr_i \rightarrow refr_{i+1}$ (i = 1, 2,…14); $refr_{15}$ → *excitable*. These state change rules say, in effect, that a firing cell goes through a determined period of refractoriness, during which it cannot be forced to fire again, either by inputs from other cells or by a spontaneous event. The *second* part concerns the possibilities for an *excitable* cell: (a) if any cell connected to an *excitable* cell is *firing* at time step *t*, then the *excitable* cell → *firing* at time step t + 1; (b) if a *spontaneous event* occurs (see below), then the excitable cell fires at the next time step; (c) otherwise, the cell simply remains *excitable*. With respect to condition (a), what this means is that the probability of propagation of spike from one axon to another is unity, provided that the second axon is not already firing and is not refractory. In preliminary simulations (not shown), we checked that if the propagation probability is less than unity (but not too small), then network frequency is not systematically altered; but we did not pursue this question as regards spatial characteristics of the oscillations.

The spontaneous events are characterized by a single parameter, p_{spon}, the probability that an excitable cell fires spontaneously on a given time step. A typical value of p_{spon} would be 1/80,000: This value would imply that an excitable cell fires—on its own—an average of once every 20 s.

To summarize the basic parameters: If the array dimensions are fixed (which also determines the total number of cells), and the rules for state transitions are fixed, then the three basic parameters are: <i> (the mean index, which may also be specified by stating the total number of gap junctions in the network); c_r, which determines how localized the connections are in space; and p_{spon}.

Simulations were run in either of two modes: first, p_{spon} was set to 0, and a single cell set to *firing*, while all other cells were *excitable*. In this way, one could observe the behavior of a single wave of activity, unperturbed by other waves. Alternatively, all cells were initialized as *excitable*, with p_{spon} at some fixed nonzero value. In this way, spontaneous activity was simulated, for up to 8,192 time steps. The following quantities were stored: the total number

of *firing* cells, in the whole array, and in each of 48 equal-sized square subarrays, in a 6 × 8 arrangement (to match the sub-dural grid layout used for the illustrated patient data). For making videos of the activity, the locations of firing cells were stored, every 2–5 time steps; however, to make the images intelligible, only every fourth or every sixth firing cell was saved. When only a single wave was studied, the computer saved the following quantities as functions of time: the total number of firing cells, the mean distance of all firing cells from the initially firing cell, and the standard deviation of this latter quantity. Long runs of spontaneous activity were also analyzed with a fast Fourier transform algorithm.

Results

Patient characteristics

Patient B was an 11-year old boy with mild learning difficulties and multiple daily seizures from soon after birth. Seizures consisted of a brief stare or a tonic fall, extension of the arms, cyanosis, and then clonic movements, particularly of the right arm. There was postictal right-sided weakness that became persistent by the age of 10. There were also involuntary movements and acquired speech difficulties. Anticonvulsant medications at the time of intracranial EEG assessment consisted of carbamazepine and chlormethiazole. An MRI scan showed an abnormality of gyral patterning in the left inferior frontal gyrus posteriorly.

Surface EEG ictal recordings in Patient B supported an origin in the left hemisphere. Ictal single-photon emission computed tomography (SPECT) showed hyperperfusion over the left lateral frontal cortex in the region of the abnormal cortical gyration. Placement of the subdural grid was guided by reconstruction of the cortical surface with projection of the region of SPECT hyperperfusion. The 6 × 8 contact grid was inserted following a left frontotemporal craniotomy, in August 2003. Sixty-five hours of video-EEG recording were obtained, including nine typical seizures. Seizure onset consisted of low-amplitude very fast activity at contacts 36–37 (eight seizures), or 36 alone (one seizure). There was consistent spread toward contact 15, with early involvement of contacts 30–32 within 2 s. There was spread of activity across the grid at the time of clinical spasms and arm extension. Electrical stimulation with 20-Hz trains of biphasic stimulation of up to 3 mA for 3 s was carried out at contacts 9–48; this did not induce any electrical or clinical seizures.

On removal of the subdural grid, cortex underlying contacts 36–39, 28–31, and 21–22 was excised down to the insula (left posterior frontal resection). Initial seizure freedom with improved deficits was not maintained beyond 8 months postoperatively. Repeated ictal SPECT again demonstrated hyperperfusion anterior to the original resection. SPECT was coregistered with postoperative 3D MRI, guiding a further resection in January 2006. Since then, the patient has been seizure-free, with improved speech (despite the left posterior frontal resection), and with no motor deficits. Neuropathology for both cortical resections showed subpial gliosis, without cortical dysplasia.

The other patient was investigated at age 13 months. She had a posterior right frontal cortical dysplasia. Her seizures included behavioral arrest, a tonic phase, and left-sided and also generalized jerking movements; further details are given in Traub et al. (2001). The spatiotemporal patterns of VFOs were similar in both patients.

Temporal features of VFOs in Patient 1

Electrographic seizures in both patients were preceded by runs of VFOs lasting hundreds of milliseconds to several seconds. An example is shown in Fig. 1A. This VFO was typically seen in all subdural electrodes immediately prior to seizure onset, but with power differences favoring the presumed seizure-onset zone (see Roopun et al., 2009). Spectral analysis of short

epochs of VFOs (400–600 ms) revealed multiple frequencies, as reported in other studies (e.g., Staba et al., 2002). In the current study, activity was seen at two predominant frequencies: 76 ± 8 and 132 ± 12 Hz (Fig. 1A). The seizure discharge in Fig. 1A lasted >7 min.

Very fast oscillations occur in intrinsically bursting pyramidal cell networks, in layer 5 of temporal neocortex in vitro, in "non-synaptic" alkaline conditions, associated with somatic spikelets

We also observed runs of VFOs in layer 5 of rat temporal neocortex in vitro, when (1) phasic synaptic currents were pharmacologically blocked (with SYM2206 for AMPA, APV for NMDA, and gabazine for $GABA_A$); (2) the slice was activated with submicromolar kainate (400 n_M); (3) alkaline aCSF was pressure-ejected nearby, in an attempt to open gap junctions (Spray et al., 1981). An example is shown in Fig. 1B. Intracellular recording of a layer 5 IB neuron revealed spikes and spikelets (fast prepotentials) that were phase-locked to the very fast oscillating field potential (130 Hz in the illustrated example, 118 ± 10 Hz, n = 5, on average). Full spike and spikelet times were quantified with respect to peak negativity on each VFO field potential wave. The graph (right) shows a pooled incidence plot (bin width 0.5 ms) for 500 field potential VFO periods, with full spike data plotted as the gray line and spikelet data as the black line, demonstrating both spikes and spikelets locked to the field. (Note the near threefold excess of spikelets versus spikes in this field potential–determined time window.)

Spikelets were more likely to occur than full action potentials when the membrane was relatively hyperpolarized (c.f. Fig. 3 of Cunningham et al., 2004; and Schmitz et al., 2001), consistent with an axonal origin of the spikelets. A strikingly similar pattern of field and intracellular activity was seen in detailed network simulations (Fig. 1B, lower right), where model pyramidal cells were coupled by axonal gap junctions, and chemical synapses were absent. Again, spikelets were more common than full action potentials at relatively hyperpolarized somatic membrane potentials; in the model it was possible to show that each somatic spikelet corresponded to an axonal action potential (not illustrated). Therefore, in the model, pyramidal cell axons fired full spikes that were phase-locked to the field. [Note as well that in our experimental conditions, kainate is expected to induce a slow depolarization in principal neurons (Fisahn et al., 2004); and with kainate receptors tonically activated, they are not available to mediate fast oscillations.]

Comment on rationale for the cellular automaton model

The data in Fig. 1 define the rationale for the way we use the cellular automaton model to represent VFOs. The rationale is based on two hypotheses: (1) that VFOs in epileptic neocortex are generated by similar mechanismsto those operative in the in vitro conditions used in Fig. 1B; and (2) that VFOs are generated by networks of axons that are electrically coupled by gap junctions. Therefore, each "cell" in the cellular automaton model represents an axon, rather than a cell body, and the interactions between "cells" represent gap junctions, rather than chemical synapses. Specifically, in Fig. 1B, excitatory and fast inhibitory chemical synapses have been blocked. Furthermore, the time step for spike propagation from cell to cell, in the model corresponding to 0.25 ms, is much smaller than expected to occur for excitatory synapses between pyramidal cells (Miles & Wong,1986).

Spatial patterns of VFOs in a patient and corresponding patterns in cellular automaton model

When spatial patterns of VFOs are inspected by eye, a common principle is immediately apparent, in every cycle: At a given time, a "blob" or "blobs" of activation might be present. The blobs move about and expand, and when they touch, they coalesce. In addition, at times and places of little activation, a "blob" would emerge, as if from nowhere, and then expand. The spatial pattern of one cycle of VFO, from ECoG recording, is illustrated in the left column

of Fig. 2. Qualitatively similar patterns of activity were seen in model VFO (Fig. 2, right column), provided there was a spatial constraint on gap junctional connectivity, and not otherwise. [Supporting Information contains videos of patient and simulation data, which allow comparison of spatial patterns over a large number of waves.) An analysis of why the cellular automaton model behaves in this way, when connectivity is spatially constrained, is provided in the Appendix S1 (Supporting Information), but the next figure illustrates the main point.

In the model, defined propagation of activity requires that gap junctions occur between nearby neurons

Fig. 3 illustrates a property of wave propagation in the cellular automaton model, as the connectivity parameter c_r is varied; in each case, a single cell was activated, and there was no other spontaneous activity. Waves of activation developed (see Appendix S1, Supporting Information), and the propagation pattern can be comprehended in terms of the mean distance of activated cells, from the starting cell, as a function of time. Therefore, for example, when connectivity is extremely localized, say with $c_r = 10$, the wave spreads slowly; the wave is also quite narrow (not illustrated). As c_r increases, wave velocity increases (and the waves become broader), until finally wave propagation begins to break down ($c_r = 50$). When there is no localization of connections at all ($c_r = \infty$), and activity can jump from anyplace to anyplace, then of course waves are not defined, and one does not see spatial features, or “blobs.” Thus as intuitively expected, the existence of spatial structure implies localization of the connections.

Discussion

The main conclusion is that preseizure ECoG VFO is characterized not only by its frequency and duration, but also—at least in some patients—by spatial patterning. The patterns have two key features: *first*, the patterns suggest spreading waves of activation, and similar patterns can be seen in a model based (somewhat abstractly) on the idea of electrical coupling between nearby pyramidal cells. In vivo field and intracellular data are also consistent with this concept. *Second*, each wave is initiated by activity within a localized cortical region. The model replicates this feature as well.

Before entering into a deeper analysis of the features and predictions of the cellular automaton model, let us first discuss why the present results are of clinical relevance. Very fast oscillations, in ECoG and depth EEG recordings, have been amply documented prior to seizures, with a small sample of references including these: Fisher et al. (1992); Bragin et al. (1999a,b, 2002); Jacobs et al. (2008); Khosravani et al. (2009); Worrell et al. (2004); Traub et al. (2001). It is even conceivable that the occurrence of VFOs prior to seizures is “generic,” that is, characteristic of all or virtually all seizure events. Such data make it imperative for epileptologists to consider a number of interrelated questions, including these: (1) what cellular events does VFO represent? (2) Why does VFO occur before a seizure, and what causal relation might it have with the subsequent seizure? (3) What is the significance of the fact that VFO is experimentally produced, most readily, when a number of phasic synaptic conductances are suppressed, and how might such conditions arise in situ? (4) In patients, are interventions targeted to VFO possible or desirable? It is crucial to understand the physiologic and spatiotemporal relationship of VFO to seizure onset in order not only to determine the role of VFOs in the development of seizures, but also the potential value of VFOs for presurgical localization. Understanding the cellular mechanisms of VFOs will be useful for addressing the clinical issues.

Although the present study obviously does not address all of these questions, we have provided further in vitro and modeling data supporting the notion that VFOs are generated by electrically coupled networks of principal neurons, via gap junctions; and we have produced a model that can specifically and testably account for both the temporal and (now) the spatial features of

VFOs. As far as we are aware, our model is the only one available that accounts for both temporal and spatial features of VFO, in a manner consistent with experimental data.

What our model does not yet account for is the likelihood that, in the brain in situ, synaptic conductances are unlikely to be suppressed to the extent that they are in our in vitro experimental conditions (Fig. 1). (A side implication of this is that VFOs measured by ECoG most likely are produced by a combination of synaptic currents and population spikes, whereas the in vitro data in Fig. 1 represent mostly population spikes.) Further analysis of this issue will require additional in vivo data, better defining the actual properties of chemical synaptic conductances (as well as gap junctions) under the conditions when VFOs occur. In the meantime, it is our opinion that our VFO model is sufficiently compelling to have concrete clinical implications, specifically that seizure onset is somehow related to the opening of gap junctions between principal neurons. This argues for studies to determine the empirical spatiotemporal relationship between VFOs and seizure onset zones (as currently defined), and for more effort to be dedicated to developing agents that modify conductance at gap junctions as potential anticonvulsants.

A deeper understanding of the implications of the cellular automaton model requires some more detailed consideration of its structural features. The dynamical behavior of the model, as a physical system, is described in the Appendix S1 (Supporting Information).

Comparison of the number of cells in the cellular automaton model, with the number of cells contributing to VFOs in the subdural grid array

For most simulations with our model, we have used up to 480,000 cells, or roughly 5×10^5. In the cortex, our data (Fig. 1) suggest that VFOs are generated in layer 5 by electrical coupling, without a requirement for chemical synapses. A separate study (Roopun et al., 2006) has shown that networks of IB tufted layer 5 pyramids, electrically coupled via gap junctions, can generate beta2 (20–30 Hz) oscillations. As a preliminary hypothesis, therefore, we suggest that VFOs might also be generated by electrically coupled layer 5 IB neurons. If that is the case, then we ask: How many layer 5 IB neurons contribute to the oscillations recorded across the subdural grid, and how does that number compare with the number used in the model? It is possible to make a rough estimate as follows: With an interelectrode spacing of 1 cm, an 8 × 6 grid would cover about 35 cm^2 on the brain surface; allowing for cortex buried in sulci, as much as 100 cm^2 (or 10^4 mm^2) of cortical surface area might be contributing to the potentials measured. O'Kusky and Colonnier (1982) reported that 1 mm^2 of macaque monkey visual cortex covered 54,000 neurons in layers 5 and 6. Let us then estimate about 10^4 layer 5 IB cells per mm^2 of cortical surface. Therefore, something like 10^8 layer 5 IB neurons might be contributing to potentials measured across the subdural grid, roughly 200 times as many cells used for most simulations in the model, and about 20 times as many cells as used in the 3D model.

Does this estimated difference in scale detract from the usefulness of the model? On physical grounds, we suspect not: The oscillation frequency in the model is independent of scale (see Appendix S1), at least over the range and in the conditions we have studied it, and the properties of wave interaction that we illustrate will also be independent of scale. There are three means by which this idea can be further tested: (1) using massive cellular automaton simulations (i.e., with tens of millions of cells) on a parallel computer; (2) performing measurements of spatial patterns of VFOs in the cortex, using devices with smaller interelectrode distances, to determine if wave interactions on a fine scale look similar to interactions on a larger scale; (3) testing specific predictions of the present model. We shall consider below item (3), as the other two items remain for future research. [We have, however, performed preliminary simulations in a cellular automaton model with 5.76 million cells, as described in Methods, with a 3D array of dimensions 1,600 × 1,200 × 3; the qualitative behavior of this larger model is similar to that reported in the Appendix S1.]

The preceding estimates also allow us to make the lattice spacing in the model correspond to a physical distance, although one cannot do this precisely owing to cortical folding. One can estimate, however, that the 800 lattice spacing×axis of the 480,000-cell array (see Methods) maps onto at least a 4 cm length of cortex, so that one lattice space corresponds to 50 μm at least, and perhaps to 100 μm. The length scale c_r of 25 that we typically use would then correspond to about 1.25–2.5 mm; the value of cr = 10 lattice spacings, which also yields propagating waves (Fig. 3), could correspond to physical distance scales of about 0.5–1.0 mm. Evidence exists suggesting that epileptiform activity can be initiated in human cortex by regions as small as this (Worrell et al., 2008; Schevon et al., 2008). The above argument does not, however, allow for layering of pyramidal cells (that is, layer 5 pyramidal cells do not all lie in a 2d sheet as do most model neurons). If one allows for layering of the neurons, then the physical separation—in a plane parallel to the pia–corresponding to a given value of c_r would be somewhat larger. On the other hand, the very large 3D model generates respectable wave patterns with c_r equal to 10, or even less (not shown).

Specific model predictions

There are three specific predictions of our VFO model:

1. Very fast cortical oscillations prior to seizures depend on gap junctions;
2. the requisite gap junctions are between the axons of pyramidal neurons, most likely in layer 5;
3. gap junctions are localized, in the sense that neurons whose cell bodies are far enough apart are unlikely to be coupled (this prediction is not trivial—axonal gap junctions could conceivably be located between synaptic terminals or nodes of Ranvier, far from the cell body).

How can these predictions be tested?

Prediction 1 has been partially tested by Grenier et al. (2003), who found ~100 Hz cortical oscillations prior to electrographic seizures in anesthetized cats, which were blocked by halothane. Further studies could be done in this preparation, for example, hyperventilating the animals, inducing metabolic acidosis or alkalosis combined with measurement of brain pH (Javaheri et al., 1981), or testing the effects of carbenoxolone applied to the cortical surface or dialyzed into the cortex. [Carbenoxolone has already been shown to suppress cerebellar cortical VFOs in vivo (Servais et al., 2005).]

Predictions 2 and 3 are interrelated and can be discussed together. If cortical VFO in vivo is indeed dependent on gap junctions, then one could examine whether cortical VFO persists in a connexin36 knockout mouse, in which electrical coupling between interneurons is greatly reduced, but in which hippocampal VFO still persists (Hormuzdi et al., 2001). It is already known that VFO in hippocampal slices in low calcium media, which is generated by pyramidal neurons (Draguhn et al., 1998), is indistinguishable between wild-type mice and connexin36 knockout mice (Hormuzdi et al., 2001). Observation of *cortical* VFO in connexin36 knockout mice, in vivo, would strongly suggest that the oscillation is generated by principal neurons, and not by interneurons.

The axon initial segments of layer 5 pyramidal cells (in ferret prefrontal cortex) are unmyelinated for hundreds of microns, even up to about 1 mm (Shu et al., 2007). Although this property may not be typical of all layer 5 pyramids, in all cortical regions and in all species, it does suggest that the spatial scale for coupling pyramidal cells could be on the order of 2 mm, at most. This figure is at least roughly in accord with the scaling of our model (see above). On the other hand, definitive demonstration of, and localization of, gap junctions on pyramidal cell axons will probably require freeze fracture replica immunogold labeling (FRIL) (Hamzei-

Sichani et al., 2007); this remains to be accomplished, and may prove a daunting task. The clinical stakes are, however, high, in our opinion.

Supplementary Material

Refer to Web version on PubMed Central for supplementary material.

Acknowledgments

Supported by NIH/NINDS (R01NS044133 to RDT), the Alexander von Humboldt Stiftung, IBM Corp., MRC Milstein Fund (United Kingdom), The Wolfson Foundation, The Royal Society and the Newcastle upon Tyne Healthcare Charities Trust. The content is solely the responsibility of the authors and does not necessarily reflect the official views of the National Institute of Neurological Disorders and Stroke or the National Institutes of Health. We thank Drs. Lawrence S. Schulman and Erin Munro for helpful discussions.

We confirm that we have read the Journal's position on issues involved in ethical publication and affirm that this report is consistent with those guidelines.

References

Bragin A, Engel J Jr, Wilson CL, Fried I, Buzsáki G. High-frequency oscillations in the human brain. Hippocampus 1999a;9:137–142. [PubMed: 10226774]

Bragin A, Engel J Jr, Wilson CL, Fried I, Mathern GW. Hippocampal and entorhinal cortex high-frequency oscillations (100–500 Hz) in human epileptic brain and in kainic acid-treated rats with chronic seizures. Epilepsia 1999b;40:127–137. [PubMed: 9952257]

Bragin A, Mody I, Wilson CL, Engel J Jr. Local generation of fast ripples in epileptic brain. J Neurosci 2002;22:2012–2021. [PubMed: 11880532]

Cunningham MO, Halliday DM, Davies CH, Traub RD, Buhl EH, Whittington MA. Coexistence of gamma and high-frequency oscillations in the medial entorhinal cortex *in vitro*. J Physiol 2004;559:347–353. [PubMed: 15254156]

Draguhn A, Traub RD, Schmitz D, Jefferys JGR. Electrical coupling underlies high-frequency oscillations in the hippocampus *in vitro*. Nature 1998;394:189–192. [PubMed: 9671303]

Engel J Jr, Bragin A, Staba R, Mody I. High-frequency oscillations: what is normal and what is not? Epilepsia 2009;50:598–604. [PubMed: 19055491]

Erdös P, Rényi A. On the evolution of random graphs. Publ Math Inst Hungar Acad Sci 1960;5:17–61.

Fisahn A, Contractor A, Traub RD, Buhl EH, Heinemann SF, McBain CJ. Distinct roles for the kainate receptor subunits GluR5 and GluR6 in kainate-induced hippocampal gamma oscillations. J Neurosci 2004;24:9658–9668. [PubMed: 15509753]

Fisher RS, Webber WRS, Lesser RP, Arroyo S, Uematsu S. High-frequency EEG activity at the start of seizures. J Clin Neurophysiol 1992;9:441–448. [PubMed: 1517412]

Gonzáles-Nieto D, Gómez-Hernández JM, Larrosa B, Gutiérrez C, Muñoz MD, Fasciani I, O'Brien J, Zappalà A, Cicirata F, Barrio LC. Regulation of neuronal connexin-36 channels by pH. Proc Natl Acad Sci U S A 2008;105:17169–17174. [PubMed: 18957549]

Grenier F, Timofeev I, Steriade M. Focal synchronization of ripples (80–200 Hz) in neocortex and their neuronal correlates. J Neurophysiol 2001;86:1884–1898. [PubMed: 11600648]

Grenier F, Timofeev I, Steriade M. Neocortical very fast oscillations (ripples, 80–200 Hz) during seizures: intracellular correlates. J Neurophysiol 2003;89:841–852. [PubMed: 12574462]

Gutnick MJ, Lobel-Yaakov R, Rimon G. Incidence of neuronal dye-coupling in neocortical slices depends on the plane of section. Neuroscience 1985;15:659–666. [PubMed: 3906427]

Hamzei-Sichani F, Kamasawa N, Janssen WGM, Yasamura T, Davidson KGV, Hof PR, Wearne SL, Stewart MG, Young SR, Whittington MA, Rash JE, Traub RD. Gap junctions on hippocampal mossy fiber axons demonstrated by thin-section electron microscopy and freeze-fracture replica immunogold labeling. Proc Natl Acad Sci U S A 2007;104:12548–12553. [PubMed: 17640909]

Hormuzdi SG, Pais I, LeBeau FEN, Towers SK, Rozov A, Buhl EH, Whittington MA, Monyer H. Impaired electrical signaling disrupts gamma frequency oscillations in connexin 36-deficient mice. Neuron 2001;31:487–495. [PubMed: 11516404]

Jacobs J, LeVan P, Chander R, Hall J, Dubeau F, Gotman J. Interictal high-frequency oscillations (80–500 Hz) are an indicator of seizure onset areas independent of spikes in the human epileptic brain. Epilepsia 2008;49:1893–1907. [PubMed: 18479382]

Javaheri S, Clendening A, Papadakis N, Brody JS. Changes in brain surface pH during acute isocapnic metabolic acidosis and alkalosis. J Appl Physiol 1981;51:276–281. [PubMed: 7263434]

Khosravani H, Mehrotra N, Rigby M, Hader WJ, Pinnegar CR, Pillay N, Wiebe S, Federico P. Spatial localization and time-dependent changes of electrographic high frequency oscillations in human temporal lobe epilepsy. Epilepsia 2009;50:605–616. [PubMed: 18717704]

Lewis TJ, Rinzel J. Self-organized synchronous oscillations in a network of excitable cells coupled by gap junctions. Network: Comput Neural Syst 2000;11:299–320.

Mercer A, Bannister AP, Thomson AM. Electrical coupling between pyramidal cells in adult cortical regions. Brain Cell Biol 2006;35:13–27. [PubMed: 17940910]

Miles R, Wong RKS. Excitatory synaptic interactions between CA3 neurones in the guinea-pig hippocampus. J Physiol 1986;373:397–418. [PubMed: 3018233]

Nimmrich V, Maier N, Schmitz D, Draguhn A. Induced sharp wave-ripple complexes in the absence of synaptic inhibition in mouse hippocampal slices. J Physiol 2005;563:663–670. [PubMed: 15661820]

O'Kusky J, Colonnier M. A laminar analysis of the number of neurons, glia, and synapses in the adult cortex (area 17) of adult macaque monkeys. J Comp Neurol 1982;210:278–290. [PubMed: 7142443]

Pytte E, Grinstein G, Traub RD. Cellular automaton models of the CA3 region of the hippocampus. Network 1991;2:149–167.

Roopun A, Middleton SJ, Cunningham MO, LeBeau FEN, Bibbig A, Whittington MA, Traub RD. A beta2-frequency (20–30 Hz) oscillation in non-synaptic networks of somatosensory cortex. Proc Natl Acad Sci U S A 2006;103:15646–15650. [PubMed: 17030821]

Roopun AK, Traub RD, Baldeweg T, Cunningham MO, Whittaker RG, Trevelyan A, Duncan R, Russell AJC, Whittington MA. Detecting seizure origin using basic, multiscale population dynamic measures: preliminary findings. Epilepsy Behav 2009;14 suppl 1:39–46. [PubMed: 18834957]

Roopun AK, Somonotto JD, Pierce ML, Jenkins A, Schofield I, Kaiser M, Whittington MA, Traub RD, Cunningham MO. A non-synaptic mechanism underlying interictal discharges in human epileptic neo-19 cortex. (in prep.).

Sarkar P. A brief history of cellular automata. ACM Computing Surveys 2000;32:80–107.

Schevon CA, Ng SK, Cappell J, Goodman RR, McKhann G Jr, Waziri A, Branner A, Sosunov A, Schroeder CE, Emerson RG. Microphysiology of epileptiform activity in human neocortex. J Clin Neurophysiol 2008;25:321–330. [PubMed: 18997628]

Schmitz D, Schuchmann S, Fisahn A, Draguhn A, Buhl EH, Petrasch-Parwez RE, Dermietzel R, Heinemann U, Traub RD. Axo-axonal coupling: a novel mechanism for ultrafast neuronal communication. Neuron 2001;31:831–840. [PubMed: 11567620]

Seiden PE, Schulman LS, Gerola H. Stochastic star formation and the evolution of galaxies. Astrophys J 1979;232:702–706.

Servais L, Bearzatto B, Schwaller B, Dumont M, De Saedeleer C, Dan B, Barski JJ, Schiffmann SN, Cheron G. Mono- and dual-frequency fast cerebellar oscillation in mice lacking parvalbumin and/or calbindin D-28k. Eur J Neurosci 2005;22:861–870. [PubMed: 16115209]

Shu Y, Duque A, Yu Y, Haider B, McCormick DA. Properties of action-potential initiation in neocortical pyramidal cells: evidence from whole cell axon recordings. J Neurophysiol 2007;97:746–760. [PubMed: 17093120]

Spray DC, Harris AL, Bennett MVL. Gap junctional conductance is a simple and sensitive function of intracellular pH. Science 1981;211:712–715. [PubMed: 6779379]

Staba RJ, Wilson CL, Bragin A, Fried I, Engel J Jr. Quantitative analysis of high-frequency oscillations (80-500 Hz) recorded in human epileptic hippocampus and entorhinal cortex. J Neurophysiol 2002;88:1743–1752. [PubMed: 12364503]

Traub RD, Schmitz D, Jefferys JGR, Draguhn A. High-frequency population oscillations are predicted to occur in hippocampal pyramidal neuronal networks interconnected by axoaxonal gap junctions. Neuroscience 1999;92:407–426. [PubMed: 10408594]

Traub RD, Whittington MA, Buhl EH, LeBeau FEN, Bibbig A, Boyd S, Cross H, Baldeweg T. A possible role for gap junctions in generation of very fast EEG oscillations preceding the onset of, and perhaps initiating, seizures. Epilepsia 2001;42:153–170. [PubMed: 11240585]

Traub RD, Cunningham MO, Gloveli T, LeBeau FEN, Bibbig A, Buhl EH, Whittington MA. GABA-enhanced collective behavior in neu- ronal axons underlies persistent gamma-frequency oscillations. Proc 20 Natl Acad Sci U S A 2003;100:11047–11052.

Traub RD, Contreras D, Cunningham MO, Murray H, LeBeau FEN, Roopun A, Bibbig A, Wilent WB, Higley MJ, Whittington MA. Single-column thalamocortical network model exhibiting gamma oscillations, sleep spindles and epileptogenic bursts. J Neurophysiol 2005;93:2194–2232. [PubMed: 15525801]

Wolfram, S. A new kind of science. Champaign, IL: Wolfram Media; 2002.

Worrell GA, Parish L, Cranstoun SD, Jonas R, Baltuch G, Litt B. High-frequency oscillations and seizure generation in neocortical epilepsy. Brain 2004;127:1496–1506. [PubMed: 15155522]

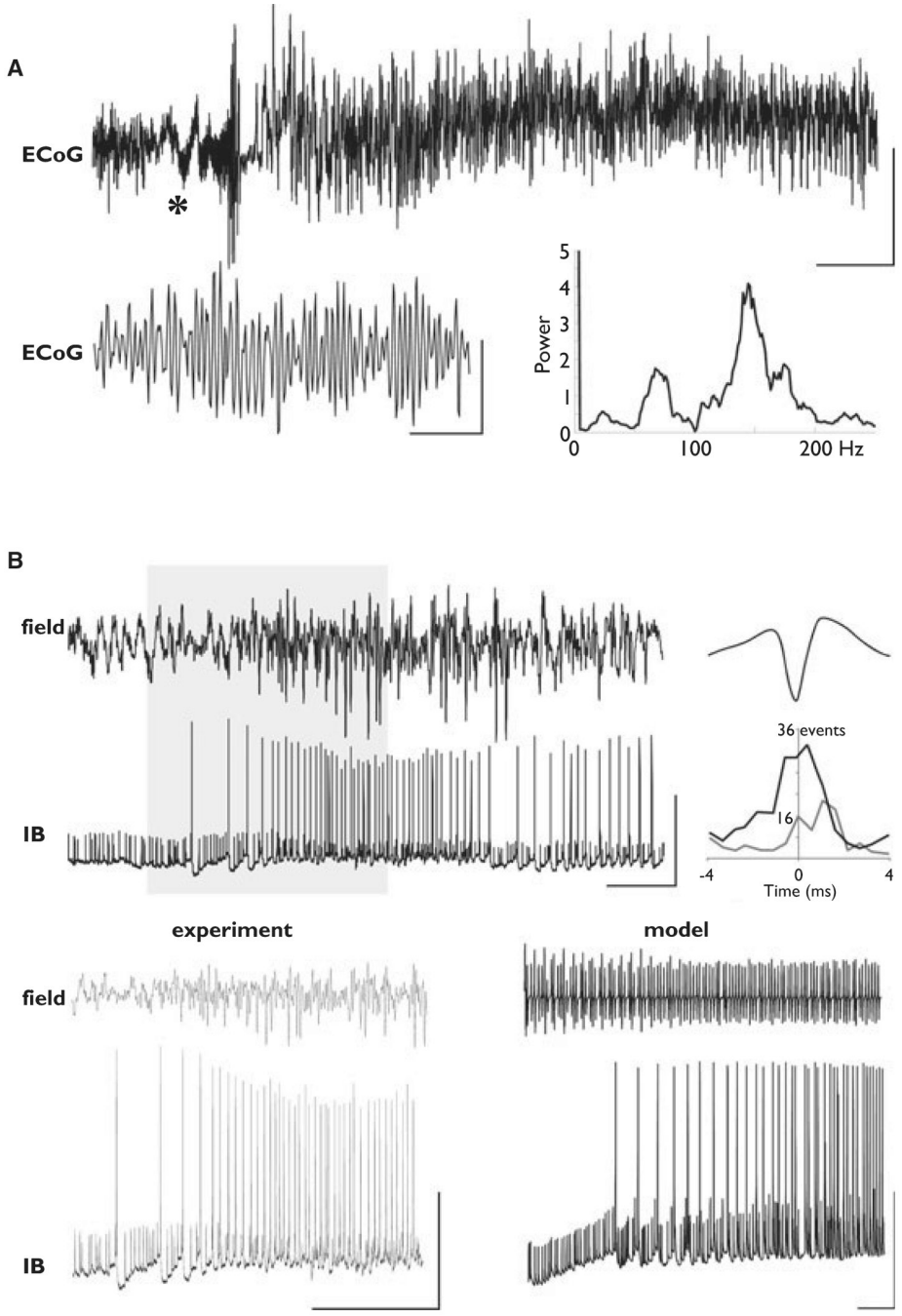

Figure. 1.

Very fast oscillations (VFOs) occur at the surface of human epileptic brain; in layer 5 of rat neocortex, in vitro, with chemical synapses blocked; and in a detailed network model of neurons coupled by gap junctions, without chemical synapses. (**A**) Electrocorticography (ECoG) recording from epileptic frontal neocortex (previously unpublished data from patient B of Roopun et al., 2009). The portion marked by "*" is expanded below. Power spectrum is from 1 s of data. Scale bars: 100 μV, 11 s; 10 μV, 100 ms. (**B**) Upper traces are field and intracellular recordings (IB, or intrinsic bursting cell), showing VFO in layer 5 of rat temporal neocortex in "nonsynaptic conditions": AMPA, *N*-methyl-D-aspartate (NMDA), and γ-aminobutyric acid $(GABA)_A$ receptors were, respectively, blocked with 21 SYM2206, AP5, and gabazine. The

bath contained kainate, and alkaline artificial cerebrospinal fluid (aCSF) was pressure ejected onto the slice just before the trace begins. Scale bars: 0.1 mV (field), 50 mV (cell), 500 ms. The graph (right) shows pooled incidence plot (bin width 0.5 ms) for 500 field VFO periods with full spike data plotted as the gray line and spikelet data as the black line. The data in the gray box were expanded in the lower left: scale bars 0.2 mV, 40 mV, and 400 ms. Simulation data are shown lower right: field potential of very fast network oscillation (above, spectral peak at 112 Hz), and simultaneous “intracellular recording” (below). Scale bars 50 mV

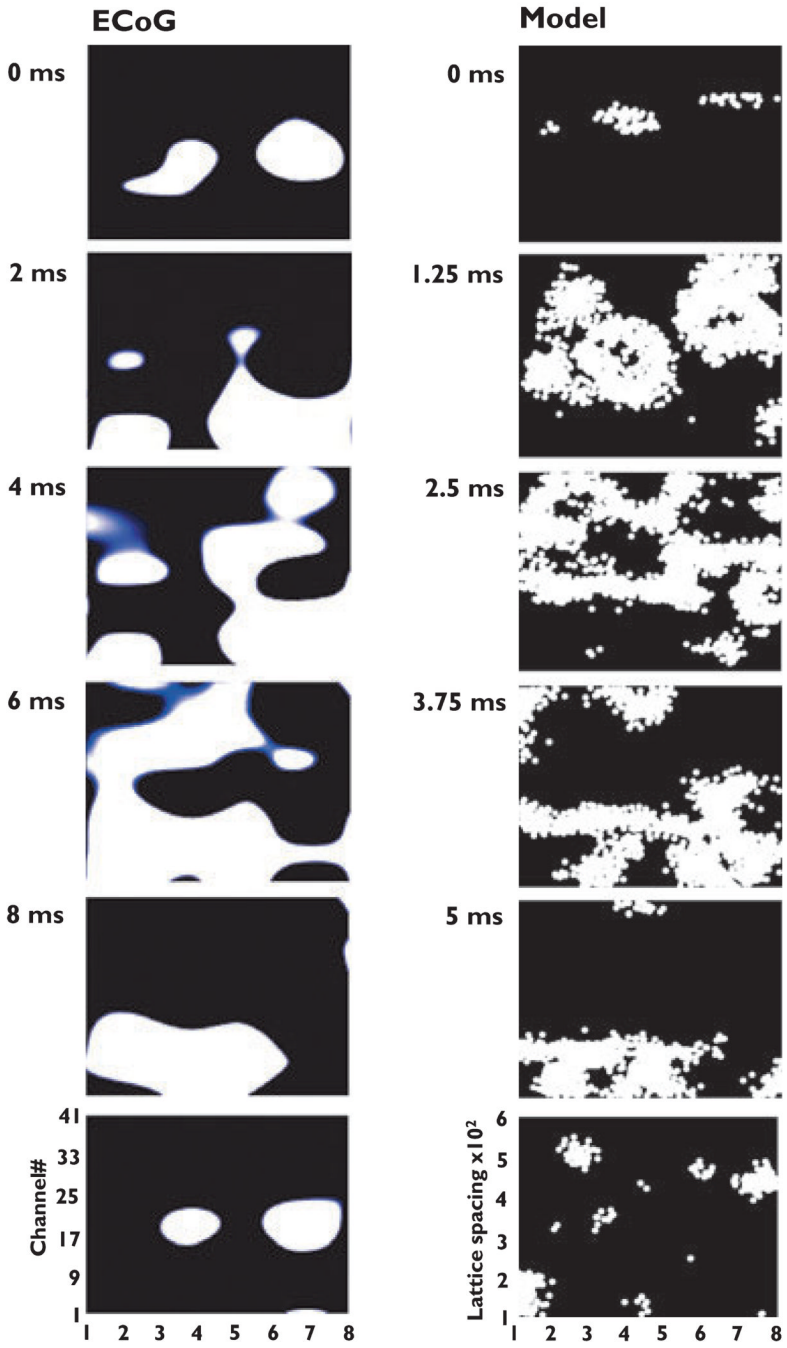

Figure. 2.

Comparison of spatiotemporal patterns in electrocorticography (ECoG) data and in cellular automaton model data. The left shows successive frames of activity, every 2 ms, from an 8 × 6 subdural array of electrodes (see Methods), in Patient B of Roopun et al. (2009). The right shows frames of activity every five time steps (i.e., every 1.25 ms) from a cellular automaton model with 480,000 cells in an 800 × 600 array, with mean index <i> 1.33, c_r = 25 lattice spacings, $p_{spon} = 1.25 \times 10^{-5}$.Videos of ongoing ECoG and model data are in Supporting Information.

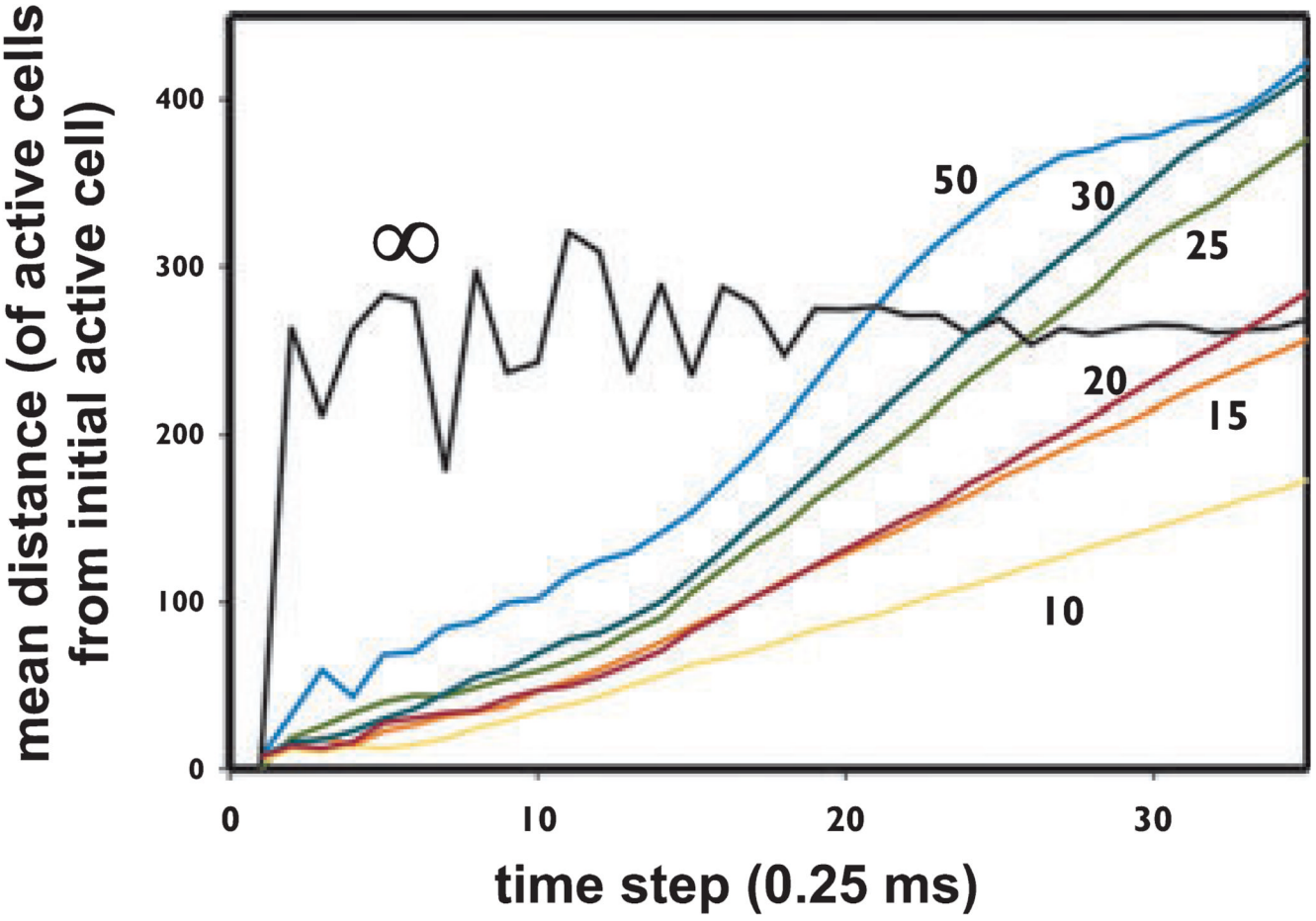

Figure. 3.

In the cellular automaton model, waves of activity propagate at constant velocity when the connectivity is localized, but not when there is global connectivity. Data are from a series of simulations with a 120,000 cell (400 × 300) model, with mean index <i> = 1.33, $p_{spon} = 0$ (i.e., no spontaneous activity), and a single starting cell activated. Over the illustrated series of simulations, the only varied quantity was c_r, the parameter which determines the maximal spacing between connected cells (see Methods). When c_r was ≤ ~35 lattice spacings, waves propagated linearly in time (after the initial growth phase), with velocity increasing as c_r increased: the more localized the connections, the slower the velocity. When c_r approached the dimensions of the array (e.g., $c_r = 50$), the distance curve becomes sigmoidal. When connectivity is not localized at all ($c_r = \infty$), there is no wave propagation: instead, the mean distance immediately jumps to the average distance, although with statistical fluctuations when activity levels are low (i.e., in the first ~15 time steps).